Journal of CO2 Utilization 75 (2023) 102564

Contents lists available at ScienceDirect

Journal of CO2 Utilization

journal homepage: www.elsevier.com/locate/jcou

Microwave plasma-based dry reforming of methane: Reaction performance and carbon formation

Seán Kelly [a,b,*], Elizabeth Mercer [b], Robin De Meyer [b,c], Radu-George Ciocarlan [d], Sara Bals [c], Annemie Bogaerts [b]

[a] School of Biosystems and Food Engineering, University College Dublin, Ireland
[b] Research Group PLASMANT, Department of Chemistry, University of Antwerp, Belgium
[c] Research Group EMAT, Department of Physics, University of Antwerp, Belgium
[d] Research Group LADCA, Department of Chemistry, University of Antwerp, Belgium

ARTICLE INFO

Keywords:
Microwave plasma
Plasma-based gas conversion
Carbon dioxide utilisation
Dry reforming of methane
Syngas

ABSTRACT

We investigate atmospheric pressure microwave (MW) plasma (2.45 GHz) conversion in CO_2 and CH_4 mixtures (i.e., dry reforming of methane, DRM) focusing on reaction performance and carbon formation. Promising energy costs of ~2.8–3.0 eV/molecule or ~11.1–11.9 kJ/L are amongst the best performance to date considering the current state-of-the-art for plasma-based DRM for all types of plasma. The conversion is in the range of ~46–49% and ~55–67% for CO_2 and CH_4, respectively, producing primarily syngas (i.e., H_2 and CO) with H_2/CO ratios of ~0.6–1 at CH_4 fractions ranging from 30% to 45%. Water is the largest byproduct with levels ranging ~7–14% in the exhaust. Carbon particles visibly impact the plasma at higher CH_4 fractions (> 30%), where they become heated and incandescent. Particle luminosity increases with increasing CH_4 fractions, with the plasma becoming unstable near a 1:1 mixture (i.e., > 45% CH_4). Electron microscopy of the carbon material reveals an agglomerated morphology of pure carbon nanoparticles. The mean particle size is determined as ~20 nm, free of any metal contamination, consistent with the electrode-less MW design.

1. Introduction

Plasma-based conversion of the key greenhouse gases, CO_2 and CH_4, so-called dry reforming of methane (DRM), offers promise to drive 'carbon circularity' in chemical and fuel production systems, which is important in the transition to a net zero carbon economy [1,2]. Plasma processes typically have very short start-up times, so are readily amenable to intermittent renewable electricity supplies [3], which continue to make up an increasing share of energy grids worldwide [4].

Plasma-based gas conversion of hydrocarbons has gained renewed interest recently [2,5–7], including innovations to address 'hard-to-abate' sectors where de-carbonisation and de-fossilisation are particularly challenging (e.g., aviation [8] and construction [9]). Plasma-produced 'syngas' (i.e., H_2 and CO mixture) can be used as a feedstock in synthesis methods (i.e., Fischer-Tropsch [10,11]) to produce, for instance, liquid hydrocarbons, such as kerosene, or key chemical building blocks, such as methanol [2,12]. End products could be sequestered as a non-gaseous product or combusted (i.e., releasing CO_2 again, but with generally a low to net zero carbon budget possible for the overall process). The 'circularity' of the enabled process will also depend on the source of CO_2 and CH_4 utilised, which can range from fossil natural gas, captured carbon from combustion, or biogenic sources (i.e., biogas) produced via anaerobic digestion of biomass [13].

MW surface wave plasmas, under atmospheric pressure conditions, offer the advantage of a high degree of ionisation (i.e., high levels of gas activation) and warm plasma conditions (favouring the endothermic chemistry of DRM). Furthermore, they operate without metal electrodes (i.e., advantageous in limiting energy loss to and erosion of metallic electrodes required in other reactor designs), and the plasma is formed in a simple quartz tube. In addition, employing a swirling gas flow with a surface wave plasma avoids plasma-quartz interactions, increasing the reactor's lifetime. Finally, they allow a quite large throughput due to the fairly high gas flow rates required to sustain a swirl flow (i.e., > 5 L/min) when compared with other lab-scale plasma reactor designs, such as gliding arcs, atmospheric pressure glow discharges, and spark configurations [7].

To date, only a small number of studies have focused on understanding the conversion of CO_2 and CH_4 mixtures by atmospheric

* Corresponding author at: School of Biosystems and Food Engineering, University College Dublin, Ireland.
E-mail address: sean.kelly2@ucd.ie (S. Kelly).

https://doi.org/10.1016/j.jcou.2023.102564
Received 19 June 2023; Received in revised form 3 August 2023; Accepted 8 August 2023
Available online 10 August 2023

pressure MW plasmas[2,14–18]. This is in stark contrast to the wide use of MW plasmas for pure CO_2 splitting [2,19–40] and CH_4/CO_2 co-conversion with Ar, N_2, H_2 or H_2O mixtures [41–51] on the one hand, and reports of other plasma types (like gliding arc, atmospheric pressure glow discharge, dielectric barrier discharges) for DRM [2,7,52–65] on the other hand. The reason for this is not particularly clear but may be due to the relative difficulty sustaining an atmospheric pressure MW plasma in the presence of CH_4, due to the formation of carbon particles, resulting from CH_4 dissociation, yielding challenging operational conditions.

In this report, we explore MW plasma-based DRM into syngas, measuring key performance indicators, including conversion and energy cost, selectivity towards syngas and by-products, as well as the plasma exhaust temperature. One important aspect, which we believe has been overlooked to date [15,16], is understanding the role of the small (but typically impactful) solid carbon by-product resulting from the dissociation of the CH_4 fraction. Small particles ("dust") in a plasma can act as a sink or source for (plasma) charged species, with the degree of coupling

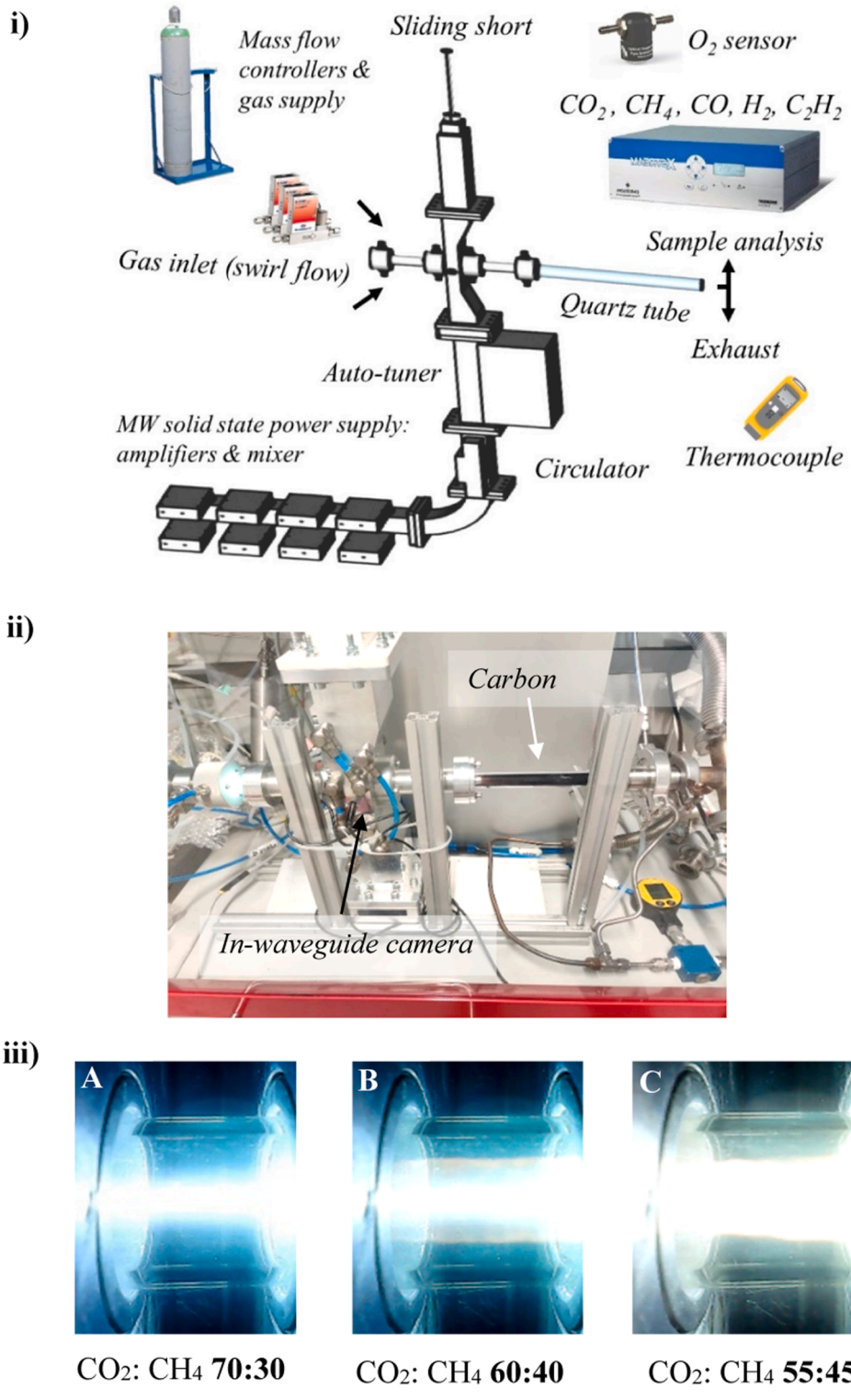

Fig. 1. **i)** Illustration of our MW plasma reactor consisting of a solid-state MW power supply, circulator, auto-tuner, and tapered waveguide section terminated by a sliding short. The plasma is ignited inside a quartz tube where a swirling flow is injected. Sample analysis of the exhaust gas is carried out using an NDIR and a luminescence O_2 sensor. **ii)** Photo of the reactor in operation for 1 kW power and 10 L/min flow rate, for a CO_2/CH_4 ratio of 55/45 with significant downstream carbon deposition on the quartz tube. Ignition takes place in a tapered section of the 2.45 GHz WR340 waveguide where a plasma is suspended at the centre of the tube. **iii)** In-waveguide photos of the plasma at different CO_2/CH_4 ratios (i.e., **A-C**) at 10 L/min. The camera viewpoint (position shown with arrow in ii)) is looking towards the quartz tube inside the waveguide. The onset of carbon formation with increasing CH_4 fraction is visible in iii) B & C, from the increased light emission at the edges surrounding the plasma filament (see text).

depending on the size, abundance, and temperature of the particulates [66–68]. Particulates can also become heated, directing energy away from plasma sustainment. In addition to its importance in maintaining a plasma, the success of any future downstream coupling of the plasma exhaust with catalyst beds (i.e., to exploit the high temperatures in the MW plasma exhaust [18]) will largely depend on the extent of 'coking' deactivation, a common hurdle for catalyst operation in DRM. Indeed, carbon formation plays a central role in industrial-scale plasma arc technologies such as the 'Hüls process' [69,70], to convert methane into hydrogen and acetylene, and the 'Kværner process' [70,71] for methane pyrolysis to generate carbon black and hydrogen. Therefore, in this paper, we study DRM in atmospheric pressure MW plasma, with special focus on carbon formation. Our work gives original insight into the impact of solid carbon formation on plasma-based DRM, which has not been the focus of previous research [2,14–18]. Further to this, we include characterisation of the produced carbon, as well as a novel quantification of water formation (a key by-product) in MW plasma-based DRM via an atom balance analysis which, to the best of our knowledge, has not previously been carried out.

2. Experimental details and analysis

In Fig. 1i) we present a schematic of our experiment. A photo is shown in Fig. 1 ii). The plasma reactor is powered by a solid-state 2.45 GHz MW source composed of a collection of power amplifiers (based on laterally diffused metal-oxide semiconductor (LDMOS) technology) from which the output powers are combined in a waveguide (WR340). This waveguide is connected via an isolator and an auto-tuner to a tapered waveguide section, including a 16 mm inner diameter quartz tube. The latter is mounted perpendicularly through a 20 mm coupling hole (i.e., $< 1/4$ wavelength in diameter), where the plasma ignition takes place. An auto-tuner, impedance analyser, and adjustable short are used to tune the electric field to optimal conditions for electrical breakdown and to sustain a continuously powered plasma with minimum reflected power (< 1%). The measurement of the absorbed plasma power, a key input parameter, is carried out using the Homer series auto-tuner from S-TEAM labs, using a six-port-reflectometer (SPR) method [72,73]. Gas injection ports coupled with a helical insert allow a swirl or vortex flow within the quartz discharge tube. Upon ignition, a surface wave sustained mode [74,75] is generated, with an axially elongated warm plasma filament located at the tube center, isolated from the tube walls (see Fig. 1 iii)). The temperature of the exhaust is monitored using a k-type thermocouple [76] and is found to be in a steady state after approximately 15 min post-ignition at which point gas analysis is performed (i.e., the exhaust concentrations are not changing after this time).

Analysis of the exhausted CO_2, CH_4, CO, and C_2H_2 is performed using non-dispersive infra-red (NDIR) absorption spectrometry (Rosemount X-STREAM XEGP Continuous Gas Analyser) [77]. The NDIR detector divides the gas sample between absorption and reference cells. The physical measurement is based on an opto-pneumatic technique where the IR absorption results in gas heating, which causes gas to outflow through a thin detection channel connecting the two chambers, and this is monitored by a micro-flow sensor providing the output voltage [77]. For H_2 measurement, a thermal conductivity detector (TCD) incorporated with our NDIR detector is used, which exploits the large differential of H_2 over other gases to conduct heat, along with signals from each NDIR channel for selectivity. The TCD is based on a Wheatstone bridge arrangement [77]. For O_2 detection, we use a sensor based on the luminescence of a dye excited with IR light, where O_2 quenches the luminescence and predictably changes its intensity for real-time monitoring [78]. Gas sampling is performed once the reactor reaches a steady state in terms of the exhaust temperature [79]. In addition to the internal calibration of each sensor, we perform external calibration using pre-mixed standards for several points across each sensor range.

We calculate the individual conversion of CO_2 and CH_4 considering their mole fractions $y_{i=CO_2,CH_4}$ (Eqs. E1-E2 below) with and without the plasma ignited (i.e., plasma ON/OFF). This is equivalent to the species mole fractions entering the plasma region (i.e., in = plasma OFF) and exhausted from the plasma (i.e., out = plasma ON). The percentage conversion χ_{CO_2,CH_4} (%) for each feed gas is then given by:

$$\chi_{CO_2}(\%) = \frac{y_{CO_2}(in) - \alpha \bullet y_{CO_2}(out)}{y_{CO_2}(in)} \bullet 100\% \quad (1)$$

$$\chi_{CH_4}(\%) = \frac{y_{CH_4}(in) - \alpha \bullet y_{CH_4}(out)}{y_{CH_4}(in)} \bullet 100\% \quad (2)$$

Here, α accounts for the changes in the gas composition and molar flow rate. Indeed, the conversion of CO_2 and CH_4 results in the primary products CO, H_2, and H_2O, along with smaller quantities of by-products, including C_2H_2, C_2H_4, C_2H_6 and C deposits. The formation of CO and H_2 increases the molar flow rate, i.e., change in stoichiometry (see reaction R1 in the Results and Discussion section below). On the other hand, the formation and condensation of H_2O to liquid and the formation of solid carbon result in mass loss from the gas flow. Altogether, the chemical conversion affects the gas composition and the molar flow rate. Thus, the relative mole fractions of the gas species measured in the exhausted mixture (i.e., $y_i(out)$, where $i = CO_2, CH_4$, Eqs. E1-E2) will be different from those at the inlet (i.e., $y_i(in)$) by a factor α, which depends on this change in molar flow rate [80]. The factor α in Eqs. E1-E2 is measured here by diluting the plasma exhaust with an unreactive 'probing' gas. The mole fraction changes in this probing or dilution gas for 'plasma ON' vs. 'plasma OFF' is a measure of the change in molar flow rate (i.e., due to the plasma conversion):

$$\alpha = \frac{y_{probe}(OFF)}{y_{probe}(ON)} + \beta\left(\frac{y_{probe}(OFF)}{y_{probe}(ON)} - 1\right) \quad (3)$$

The measurement of α is performed using a real-time O_2 sensor [78] where a small O_2 admixture of dilution ratio β (e.g., ~10% dilution of the gas inlet mass flow with $\beta = 0.1$) is added to the cooled exhaust for plasma ON and OFF conditions (i.e., $y_{probe} = y_{O_2}$, Eq. E3). Here the measured ratio $\frac{y_{probe}(OFF)}{y_{probe}(ON)}$ corresponds to the molar flow changes from chemical reactions while the term '$\beta\left(\frac{y_{probe}(OFF)}{y_{probe}(ON)} - 1\right)$' accounts for molar flow changes from the (probing) dilution. Notably, for small (probing) dilutions (i.e., $\beta \ll 1$) Eq. E3 is approximated as $\alpha \sim \frac{y_{probe}(OFF)}{y_{probe}(ON)}$. The use of a diluting gas probe to measure α has been previously reported in the context of plasma-based gas conversion [7,52,80]. No oxygen is found in the exhaust mixture for the conditions investigated in our work. Notably, the addition of O_2 to the cooled exhaust (i.e., removing any ignition source) is confirmed to be 'chemically inert' in the same way as probing gases such as N_2 or Ar have been previously employed [7,52,80]. Owing to the real-time nature of the gas sampling in this work, the gas expansion measurement is taken separately/sequentially to the other gas species measurements and not simultaneously as in earlier reports [7,80]. This allows for a more straightforward analysis (detailed below).

The total (or weighted) conversion allows for a direct comparison of performance between various DRM reports [81], particularly those employing different CO_2:CH_4 ratios. The total (or weighted) conversion, χ^{tot}(%), is defined as the conversion for each reactant weighted over their molar fraction in the inlet gas mixture:

$$\chi^{tot} = y_{CO_2}(in) \cdot \chi_{CO_2} + y_{CH_4}(in) \cdot \chi_{CH_4} \quad (4)$$

The energy cost (EC, either in eV/molecule or kJ/L) is expressed in terms of the total conversion χ^{tot}, the ratio of plasma power P_{plasma} (kW) to inlet gas flow rate $\varphi_{IN}(nL/\min)$ (i.e., a ratio known as the specific energy input, SEI), and the molar volume of gas under standard reference conditions (i.e., 24.05 [L/mol][7,82]). These are given as:

$$SEI\left(\frac{kJ}{L}\right) = \frac{P_{plasma}(kW)}{\varphi_{IN}(nL/\min)} \bullet 60\left(\frac{s}{\min}\right) \tag{5}$$

$$EC_{tot}\left(\frac{kJ}{L}\right) = \frac{SEI\left(\frac{kJ}{L}\right)}{\chi^{tot}} \tag{6}$$

$$EC\left(\frac{eV}{molecule}\right) = EC\left(\frac{kJ}{L}\right).24.05\left(\frac{L}{mol}\right) \bullet \frac{6.24 \bullet 10^{21}\left(\frac{eV}{kJ}\right)}{6.02 \bullet 10^{23} \quad \left(\frac{molecules}{mol}\right)} \tag{7}$$

Of particular interest for DRM is the energy cost of syngas production given by:

$$EC_{syngas}\left(\frac{kJ}{L}\right) = \frac{SEI\left(\frac{kJ}{L}\right)}{\alpha \bullet \left(y_{CO}(out) + y_{H_2}(out)\right)} \tag{8}$$

$$EC_{syngas}\left(\frac{eV}{molecule}\right) = EC_{syngas}\left(\frac{kJ}{L}\right).24.05\left(\frac{L}{mol}\right) \bullet \frac{6.24 \bullet 10^{21}\left(\frac{eV}{kJ}\right)}{6.02 \bullet 10^{23} \quad \left(\frac{molecules}{mol}\right)} \tag{9}$$

This value should be interpreted as the amount of energy needed to form a certain amount of syngas [83].

The mole fraction of H_2O formed by the plasma conversion is not directly measurable in our setup, as the liquid condenses out along the exhaust lines, with the exhaust sample dried before measurement. In order to indirectly estimate H_2O, we can consider the atom balances [52]. For the oxygen balance:

$$b_O = \frac{\alpha \bullet \left(y_{CO}(out) + 2 \bullet y_{CO_2}(out)\right)}{2 \bullet y_{CO_2}(in)} \tag{10}$$

We consider $b_O \sim 1 - y_{H_2O}(out)$ in Eq. (E10), where $y_{H_2O}(out)$ is the mole fraction of H_2O which condenses from the plasma exhaust before measurement. Notably, the approximation of H_2O here as the dominant liquid product is in line with earlier reports where sampling of the liquid fraction condensed from a similar CO_2/CH_4 plasma is found to be primarily H_2O with only faint traces of oxygenates [7]. Further, we found that O_2 is not present in the exhaust, also in line with earlier reports [7, 52]. This leaves only CO and H_2O as the primary routes for the conversion of oxygen atoms. By re-arranging Eq. E10 above, we can express the H_2O molar fraction in terms of known values:

$$y_{H_2O}(out) = 1 - \frac{\alpha \bullet \left(y_{CO}(out) + 2 \bullet y_{CO_2}(out)\right)}{2 \bullet y_{CO_2}(in)} \tag{11}$$

Selectivity provides an overview of the distribution of conversion products. The selectivity is defined as the number of atoms that end up as a product containing said atom, with respect to the number of atoms that are available from our reactants CO_2 and CH_4. The atoms in question are C, O and H. We calculate the selectivity of each atom (i.e., C, O and H) for our primary products CO, H_2 and H_2O along with minor product C_2H_2 as follows:

$$S_{C,CO} = \frac{\alpha \bullet y_{CO}(out)}{\left(y_{CO_2}(in) - \alpha \bullet y_{CO_2}(out)\right) + \left(y_{CH_4}(in) - \alpha \bullet y_{CH_4}(out)\right)} \tag{12}$$

$$S_{C,C_2H_2} = \frac{2 \bullet \alpha \bullet y_{C_2H_2}(out)}{\left(y_{CO_2}(in) - \alpha \bullet y_{CO_2}(out)\right) + \left(y_{CH_4}(in) - \alpha \bullet y_{CH_4}(out)\right)} \tag{13}$$

$$S_{O,CO} = \frac{\alpha \bullet y_{co}(out)}{2 \bullet \left(y_{CO_2}(in) - \alpha \bullet y_{CO_2}(out)\right)} \tag{14}$$

$$S_{O,H_2O} = \frac{y_{H_2O}(out)}{2 \bullet \left(y_{CO_2}(in) - \alpha \bullet y_{CO_2}(out)\right)} \tag{15}$$

$$S_{H,H_2} = \frac{2 \bullet \alpha \bullet y_{H_2}(out)}{4 \bullet \left(y_{CH_4}(in) - \alpha \bullet y_{CH_4}(out)\right)} \tag{16}$$

$$S_{H,H_2O} = \frac{2 \bullet y_{H_2O}(out)}{4 \bullet \left(y_{CH_4}(in) - \alpha \bullet y_{CH_4}(out)\right)} \tag{17}$$

$$S_{H,C_2H_2} = \frac{2 \bullet \alpha \bullet y_{C_2H_2}(out)}{4 \bullet \left(y_{CH_4}(in) - \alpha \bullet y_{CH_4}(out)\right)} \tag{18}$$

Given its importance in both the 'upstream' plasma dynamics and 'downstream' utilisation of the exhausted syngas, we characterise the solid carbon generated during conversion. To determine particle size distribution and the basic morphology, we employ scanning electron microscopy (SEM) with energy dispersive X-ray (EDX) spectroscopy (FEI Quanta 250 FEG) [84]. The carbon deposits are collected from the reactor wall and subsequently dispersed in chloroform by sonication. A drop of this suspension is left to dry either on an SEM stub prior to SEM imaging or on double sided carbon tape for EDX spectroscopy analysis. Further, Raman spectra were obtained on a Micro-Raman Horiba (Xplora Plus Microscope) equipped with a green 532 nm laser. The measurements were done at room temperature and in air atmosphere in the range of 50–4500 cm^{-1} Raman shift. The laser power was varied from 1% to 100% (not shown), while multiple spots of the sample were analysed (not shown). Finally, thermogravimetric analysis (TGA) was performed on a Mettler Toledo TGA-DSC 3 + analyser. The measurements were performed in O_2 with a flow rate of 80 mL/min., while the temperature ramped with 10 °C/min. until 1000 °C was reached. A sample of graphite powder (particle diameter of $\leq$ 20 μm, Fluka Inc.) was also measured as a benchmark for crystalline carbon.

3. Results and discussion

3.1. General considerations and plasma operating conditions

Syngas production is given by the following overall reaction:

$$CO_{2(g)} + CH_{4(g)} \rightleftharpoons 2CO_{(g)} + 2H_{2(g)} \tag{R1}$$

A competitive pathway to reaction R1 is the formation of, and (eventual) condensation to, liquid water, which results from the reaction of O atoms (formed from the splitting of CO_2) with H atoms (from the splitting of CH_4). Possible overall reaction pathways for water formation include the well-known methanation and reverse water gas shift reactions:

$$CO_{(g)} + 3H_{2(g)} \rightleftharpoons CH_{4(g)} + H_2O_{(l)} \tag{R2}$$

$$CO_{2(g)} + 4H_{2(g)} \rightleftharpoons CH_{4(g)} + 2H_2O_{(l)} \tag{R3}$$

$$CO_{2(g)} + H_{2(g)} \rightleftharpoons CO_{(g)} + H_2O_{(l)} \tag{R4}$$

Other by-products of note include C_2H_x molecules, where acetylene (C_2H_2) is typically the most prominent, especially at high CH_4 fractions. Solid carbon is typically a small (< 1%) but impactful by-product in terms of its physical effects on the plasma and the utilisation prospects downstream. A key pathway for solid carbon production is due to pyrolysis of CH_4 via stepwise formation of C_2H_6 (and H_2) and subsequent dehydrogenation of C_2H_6 to C_2H_4 and of C_2H_4 to C_2H_2 which finally dissociates to form solid carbon (and H_2) [85]. The overall reaction is given by:

$$2CH_{4(g)} \rightleftharpoons 2C_{(s)} + 4H_{2(g)} \tag{R5}$$

Another possible pathway for solid carbon production is the disproportionation of CO given by:

$$2CO_{(g)} \rightleftharpoons C_{(s)} + CO_{2(g)} \tag{R6}$$

We investigate a range of inlet mixtures approaching 50/50 CO_2/CH_4 at a fixed power of 1 kW at 2.45 GHz and a total mass flow rate of 10 L/min with a specific energy input of 6 kJ/L. Corresponding photographs of the discharge inside the waveguide center (i.e., at the ignition

point) are shown in Fig. 1 iii) The visible appearance of the plasma is clearly sensitive to the mixture fraction. At 70/30 CO_2/CH_4, the filament, suspended at the tube's center, is visually consistent with CO_2 MW plasmas previously reported [19,23,24]. The plasma region is contracted (radially) to approximately one skin depth (i.e., the characteristic penetration depth of MW energy), consistent with the plasma's dielectric properties in the surface wave plasma mode [24]. At the 60/40 mixture, we begin to see increased light emission around the filament, including an orange incandescence at the far edges. Further, carbon particles are collected more visibly in the downstream walls of the quartz tube for this mixture (as indicated in Fig. 1 ii). The increased light intensity at higher CH_4 fractions is therefore correlated with the onset of significant carbon production (resulting from the CH_4 pyrolysis side-reaction). The 'white' incandescence is associated with solid carbon temperatures exceeding 1500 K, while orange hues are associated with incandescence from cooler particulates at the edge regions surrounding the plasma filament [86]. Notably, much of carbon is observed to be 'pushed out' from the central (plasma) region, depositing on the quartz tube walls downstream [87]. At the highest stable CH_4 mole percentage (i.e., 55/45 CO_2/CH_4 in Fig. 1 iii) the (visible) light emission intensifies considerably and masks the visibility of the central plasma region. There is also a substantial increase in the downstream deposition of carbon on the quartz tube walls for this mixture (see Fig. 1 ii). At higher CH_4 fractions, e.g., 50/50 CO_2/CH_4 mixtures, the discharge becomes very luminous, unstable, and eventually extinguishes before any steady state (> 15 mins) can be reached.

Notably, previous works [15,16] on MW DRM used a higher specific energy input (i.e., 12 kJ/L [15] vs. 6 kJ/L used in this work) to achieve (stable) ignition/conversion at 50/50 CO_2/CH_4. Unfortunately, these operational conditions are beyond our reactor capabilities at present. It is clear, however, that the impact of solid carbon formation is significant on the DRM performance in MW plasmas, with a considerable increase in the SEI seemingly required to form a stable ignition for only a small change in CH_4 fraction (i.e., + 5%). Investigation of the produced carbon will be described later in this paper, but it is known that the plasma dynamics change in the presence of solid carbon, which can act as macroscopic charge carriers [66,67]. Indeed, aggregates/agglomerates of carbon particles typically acquire a negative charge in a plasma due to the high mobility of electrons, which reduces the electron density, and this could weaken the (electron) power coupling, which sustains the discharge. Further to this, carbon is known to be absorbent of MW radiation [88] which could weaken the power coupling to charge carriers (i.e., where energy is directed to heating the carbon) leading to difficulties sustaining a plasma. In our experiment, these key factors, related to onset of conditions with significant carbon formation, are possible explanations for the plasma extinguishing when the CH_4 fraction is only incrementally changed from 55/45 CO_2/CH_4 to 50/50 CO_2/CH_4.

3.2. Conversion, product formation and energy cost

The conversion results for the various CO_2/CH_4 mixtures are shown in Fig. 2i). The conversion of CH_4 is greater than CO_2 across all mixtures considered. This trend is in line with earlier reports on plasma-based DRM [7,15,16,52]. Indeed, this is explained by the smaller bond dissociation energy of C-H (4.48 eV) compared to C═O (5.52 eV). At 70/30 CO_2/CH_4, the CO_2 and CH_4 conversion is 49.4 ± 1.8% and 66.5 ± 1.7%, respectively. At 60/40 CO_2/CH_4, the conversion levels drop slightly to 46.2 ± 2.3% and 58.0 ± 1.8%, respectively, while at CO_2 /CH_4 of 55/45, the CO_2 and CH_4 conversion is 45.8 ± 2.5% and 55.2 ± 1.5%, respectively. The total (weighted) conversion is also shown in Fig. 2i) (see Eq. E4 above). It ranges from 53.5 ± 1.7% at 70/30 CO_2/CH_4 to 49.6 ± 2.1% at 55/45 CO_2/CH_4.

CO and H_2 are the main gaseous products formed, with H_2O as a significant by-product. The CO and H_2 mole percentages found in the exhaust for the 70/30 CO_2/CH_4 mixture are 41.0 ± 0.3% and 23.0 ± 0.1%. Small mole percentages of C_2H_2, ranging from 0.70 ± 0.16% to

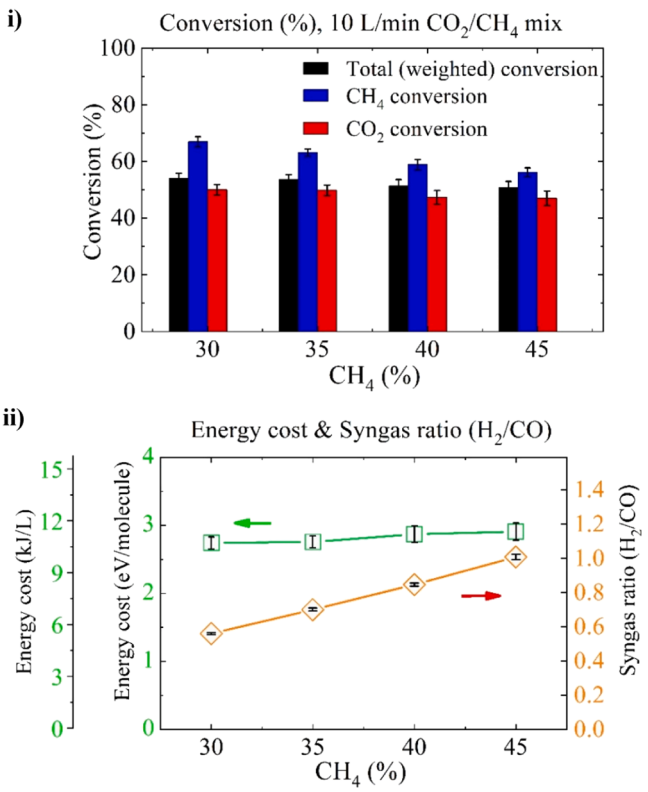

Fig. 2. i) Total conversion (weighted according to inlet fraction of CO_2 and CH_4) along with individual CH_4 and CO_2 conversion (in %) for different CH_4 content in the CO_2/CH_4 feed mixture, for an inlet flow rate of 10 L/min at 1 kW power. **ii)** Corresponding energy cost (in kJ/L and eV/molecule) shown in the left axis and syngas ratio (i.e., H_2/CO ratio) present in the exhaust shown on the right axis.

1.58 ± 0.10% for 70/30 CO_2/CH_4 to 55/45 CO_2/CH_4 are measured as well (and other C_2H_x (x = 4,6) products may also be present, but in still smaller quantities). Notably, the exhaust is found to be free of O_2 (i.e., 0%) for all conditions investigated. These trends are generally in agreement with earlier reports [7,52].

We observe significant condensation (water) in the exhaust. This is attributed to the methanation and reverse water gas shift pathways (see reactions R2–4 above). The mole percentages of H_2O are estimated here by considering the O atom balance (see Eq. E11 above), with values of 13.6 ± 3.2% at 70/30 CO_2/CH_4 and 12.1 ± 3.3% at 65/35 CO_2/CH_4, while at higher CH_4 fractions, the H_2O mole percentage is reduced to 7.2 ± 4.7% at 60/40 CO_2/CH_4 and 6.7 ± 5.2 at 65/45 CO_2/CH_4. As a sidenote, the hydrogen and carbon atom balances are potentially useful for estimation of other unknown (i.e., unmeasured) species mole fractions, such as the gaseous C2 hydrocarbons (i.e., C_2H_4 & C_2H_6) and solid carbon. These species, however, constitute a small fraction of by-products. Due to levels of uncertainty in the measured and inferred values (i.e., H_2O) needed to estimate them, an accurate determination is not currently possible. Indeed, the quantification of the solid carbon directly could be challenging as this would involve the collection of all the material deposited in the reactor for a particular run time. Further, measurements of the C2 hydrocarbons (e.g., using NDIR/UV, FTIR or GC) should consider appropriate calibration at low ranges (i.e., to minimise uncertainty).

In Fig. 2 ii) (right axis) the syngas ratio is presented. At 70/30 CO_2/CH_4, a syngas ratio of ~0.6 (0.56 ± 0.01) is obtained, while the ratio approaches ~1 (1.01 ± 0.02) at 55/45 CO_2/CH_4, consistent with greater selectivity towards H_2 (reaction R1) over H_2O (reactions R2–4).

In Fig. 2 ii) (left axis) the corresponding energy cost is given. We obtain promising energy costs ranging from 2.8 ± 0.1 eV/molecule to

3.0 ± 0.1 eV/molecule, or from 11.1 ± 0.4 kJ/L to 11.9 ± 0.5 kJ/L, for total (weighted) conversion levels of ~50–54% (i.e., 49.6 ± 2.1% to 53.5 ± 1.7%). The corresponding energy costs for syngas production (Eqs. E8 and E9) range from 1.9 ± 0.1 eV/molecule to 1.7 ± 0.1 eV/molecule, or from 7.8 ± 0.1 kJ/L to 6.9 ± 0.1 kJ/L. These total energy costs here are quite good when compared to previous works on DRM in MW plasmas (see Table 1), although at clearly lower conversion levels than [15,16]. Indeed, Zhang et al. [14] investigated atmospheric pressure MW plasma conversion using a submerged 'wire' electrode arrangement. The power was pulsed and limited to low values (~120 W); also the (mass) flow rates were limited to 200 mL/min, achieving CH_4 and CO_2 conversions of 71% and 69%, respectively, for an energy cost of 6.5 eV/molecule [2,14]. Chun et al. [15] investigated MW plasma-based DRM in a 'torch' design [89] with swirling flows of 30 L/min and powers of 6 kW (i.e., SEI ~12 kJ/L) in 50/50 CO_2/CH_4 mixtures, achieving 68% and 97% conversion for CO_2 and CH_4, respectively. This yielded an energy cost of ~3.6 eV/molecule. Under similar SEI conditions (i.e., also 12 kJ/L), Sun et al. [16] employed a surface wave MW plasma reactor design with a swirling flow arrangement at 10 L/min and 2 kW power, reporting 91% and 96% conversion for CO_2 and CH_4, respectively, and yielding an energy cost of ~3.2 eV/molecule. Another investigation by Chun et al. [17], using a different MW torch design, achieved conversion levels of 33% and 43% for CO_2 and CH_4 with swirling flows of 30 L/min and powers of 3 kW (i.e., SEI ~6 kJ/L) in 50/50 CO_2/CH_4 mixtures (without a catalyst bed). This yielded an energy cost of ~3.9 eV/molecule (see Table 1). Combinations of MW plasma and downstream catalyst beds for DRM have also been investigated. Chun et al. [17], added a Ni catalyst bed adjacent to the discharge tube, comparing this hybrid design with the non-catalytic case. Considerable gains were found with the inclusion of the downstream catalyst, as the conversion increases from 33% to 68% and from 43% to 97% for CO_2 and CH_4, respectively, compared to the non-catalytic scenario under similar conditions. This yielded an energy cost of ~2.0 eV/molecule (see Table 1). Notably, the authors reported significant issues with carbon deposition blocking the pores of the Ni nano-catalyst, leading to deactivation. Cho et al. [18] also applied a Ni catalyst, and achieved a CO_2 and CH_4 conversion of 68% and 60%, respectively, for 50:50 CO_2/CH_4 mixtures at reduced pressures (~0.04 bar) and low (mass) flow rates (100 mL/min) for powers up to 1.5 kW. The authors reported much higher energy costs in the range of 93–343 eV/molecule across different mixture ratios [2,18]. Notably the authors again reported issues with carbon deposition, leading to deactivation of the Ni catalyst employed.

In terms of energy cost, we reach slightly lower values of 2.8–3.0 eV/molecule compared to the best performance of ~3.6 eV/molecule reported by Chun et al. [15] and ~3.2 eV/molecule reported by Sun et al. [16], although typically using a lower SEI (i.e., 6 kJ/L here vs 12 kJ/L by both Chun et al. [15] and Sun et al. [16]). Notably, our energy costs are considerably lower than the earlier MW plasma DRM reports of Zhang et al. [14] consuming 6.5 eV/molecule for an SEI of 36 kJ/L. Comparing with plasma-catalytic approaches our energy cost is considerably lower than Cho et al. [18] consuming 93–343 eV/molecule for an SEI of 900 kJ/L, but higher than Chun et al. [17] consuming just 2.0 eV/molecule for an SEI of 6 kJ/L. Indeed, in this context, the incorporation of a downstream catalyst is an intriguing prospect to achieve better performance, however, as noted by Chun et al. [17] the deactivation of catalyst by carbon deposition remains a key hurdle for the viability of this approach, further motivating our study of carbon particle formations.

Snoeckx and Bogaerts [2] provided in 2017 an extensive literature overview of the state-of-the-art in the field of plasma-based DRM. They illustrated the energy cost vs. total conversion for DRM in many plasma reactors reported in the literature until that point. It should be noted that the effects of gas expansion are not described in detail in many papers, and this can lead to largely overestimated values towards conversion if not properly considered [83] (see section Experimental details and analysis above). Nevertheless, this was already corrected for in the review by Snoeckx and Bogaerts. Recently, our group has updated this overview with additional data points [7]. Here we again add our best metrics for this work, as shown in Fig. 3. Note that the y-axis is reversed, with the lowest (= best) values of the energy cost shown at the top of the

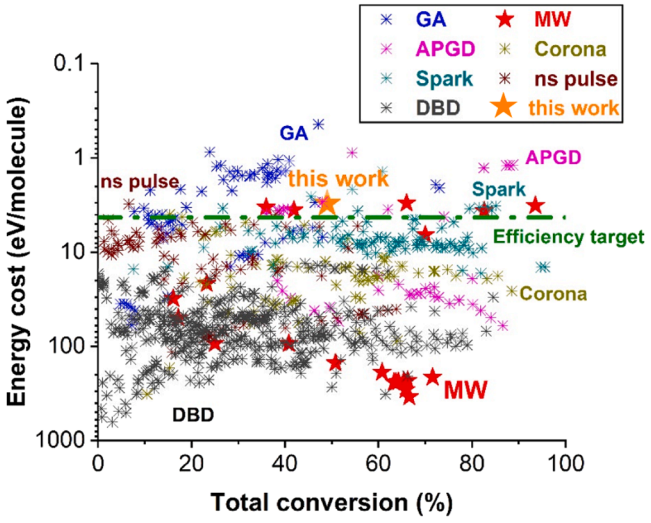

Fig. 3. Overview of energy cost (eV/molecule) vs total conversion (%), for many different plasma reactors, collected originally from literature by Snoeckx and Bogaerts [2] and updated based on more recent literature by Wanten et al. [7]. Note that the y-axis is reversed (and in log scale). The efficiency target is defined as the energy cost which should be reached to be competitive with classical DRM and emerging technologies for producing syngas (dashed line). Our own best result of 2.8 ± 0.1 eV (at 30% CH_4, 10 L/min, 1 kW) is added as an orange star.

Table 1
Comparison of typical performance metrics for MW plasma-based DRM reports to date, including this work (across different CO_2:CH_4 inlet mixture ratios). [§]inclusion of a catalyst bed.

Mass flow rate [L/min]	Pressure [atm]	Power [kW]	CO_2:CH_4 Inlet [%]	CO_2 conversion [%]	CH_4 conversion [%]	Total (weighted) conversion [%]	Energy cost [eV/molecule]	Ref.
0.2	1	0.12	40:60	71	69	70	6.5	[14]
30	1	6	50:50	68	97	83	3.6	[15]
10	1	2	50:50	91	96	94	3.2	[16]
30	1	3	50:50	33	43	38	3.9	[17]
30	1	3	50:50	69	81	75	2.0[§]	[17]
0.1	0.04	1.0	50:50	68	60	64	234[§]	[18]
10	1	1	70:30	49	67	53	2.8	This work.
10	1	1	65:35	49	63	53	2.8	This work.
10	1	1	60:40	46	58	50	2.9	This work.
10	1	1	55:45	46	55	50	3.0	This work.

axis. The efficiency target defined by Snoeckx and Bogaerts [2] reasoned that any approach achieving an energy cost under 4.27 eV would be competitive against classical DRM and competing alternatives (shown as a dashed line in Fig. 3). Notably, this target is based on the 60% energy efficiency target, defined by Snoeckx and Bogaerts for plasma technology to be competitive with the classical DRM process or other emerging technologies, for the general stoichiometric DRM process, yielding 4.27 eV per molecule [2]. Note however, that besides the energy cost, a major criterion for plasma-based DRM to become competitive with the classical DRM is how to avoid carbon deposition. Hence, in this work, we also focus on the carbon formation. Our performance is indeed clearly below this target, as all our energy cost values are between 2.8 and 3.0 eV/molecule, in the entire range of CO_2/CH_4 mixtures investigated (i.e., our data points are all above this dashed line).

Evidently from Fig. 3, there are many reactor configurations, especially the dielectric barrier discharge (DBD) reactors, which are still far above this threshold. Some of the best performing DBD reactors for DRM include reports by Wang et al. reaching an experimental conversion of 66% [90] and Snoeckx et al. reaching an energy cost at 18 eV/molecule [91]. There are several non-MW reactor types shown in Fig. 3 which do achieve promising lower energy costs. For instance, Cleiren et al. [52] achieved an energy cost of 2.5 eV/molecule for gas mixtures of CO_2 and CH_4 for a gliding arc (GA) type reactor (so-called gliding arc plasmatron (GAP) [92]), but that work only considered lower CH_4 fractions (i.e., $<$ 30% CH_4). Liu et al. [62] studied an AC pulsed 'tornado' type GA reactor and reported energy costs as low as 1.6 eV/molecule for higher CH_4 fractions, i.e., a 2/3 CH_4/CO_2 ratio. Li et al. [53] combined the GA approach with a catalyst bed for DRM, achieving an energy cost $<$ 2 eV/molecule. Small volume reactor types that also incorporate metallic electrodes, such as spark reactors [93] and atmospheric pressure glow discharges [7,55] also achieved low energy costs. Notably, these reactors are all electrode-dependent designs, a characteristic that our MW approach avoids. This electrodeless characteristic gives our approach a distinct advantage with potential benefits in terms of the longevity of operation (i.e., avoiding electrode erosion [94]) and energy costs improvements for conversion by avoiding energy loss to the reactor walls.

3.3. Product selectivity

In Fig. 4i)-iii) we present the O-, C- and H-based selectivity towards the conversion products for the different inlet mixtures (see Eqs. E12-E18 above). Syngas (i.e., CO and H_2) is the primary destination for O, C, and H atoms. Fig. 4 shows that the selectivity for syngas production improves with increasing CH_4 fraction, as the H_2O mole fractions in the exhaust mixture gradually drop.

In Fig. 4i) we observe that at 70/30 CO_2/CH_4, the O-atom selectivity towards CO and H_2O is $S_{O,CO} = 0.72 \pm 0.05$ and $S_{O,H_2O} = 0.20 \pm 0.05$. As H_2O levels drop with increasing CH_4 fraction, we observe a slightly lower selectivity towards water formation and slightly higher selectivity toward CO production, with values of $S_{O,CO} = 0.85 \pm 0.10$ and $S_{O,H_2O} = 0.14 \pm 0.11$ measured at 55/45 CO_2/CH_4. Note that the values are quite close, given the large error bars. Across this range, the cumulative selectivity is ~1 (considering the relatively large error) with values of 0.92 ± 0.07 at 70/30 CO_2/CH_4, 0.98 ± 0.13 at 60/40 CO_2/CH_4 and 0.99 ± 0.15 at 55/45 CO_2/CH_4. This is logical, given the way the H_2O mole fraction was estimated; it implies that the O-atoms are distributed primarily between CO and H_2O, except for the traces of oxygenates that are produced, considered quasi negligible, as previously discussed.

In Fig. 4 ii) the C-based selectivity towards CO and C_2H_2 for the different inlet mixtures is presented. The C-based selectivity towards CO drops slightly with increasing CH_4 fraction, from $S_{C,CO} = 0.91 \pm 0.04$ at 70/30 CO_2/CH_4 to $S_{C,CO} = 0.85 \pm 0.06$ at 55/45 CO_2/CH_4. For C_2H_2, the C-based selectivity is low, i.e., $S_{C,C_2H_2} = 0.03 \pm 0.01$ at 70/30 CO_2/CH_4, and $S_{C,C_2H_2} = 0.09 \pm 0.01$ at 55/45 CO_2/CH_4. The cumulative selectivity is ~1 (considering the relatively large error) across the range, with values of 0.94 ± 0.04 at 70/30 CO_2/CH_4, 0.97 ± 0.06 at 60/40 CO_2/CH_4 and 0.94 ± 0.06 at 55/45 CO_2/CH_4. This indicates that only a small fraction of the C atoms is likely directed towards other C_2H_x species (e.g., C_2H_4, C_2H_6) or solid carbon production, which were unfortunately not available for measurement with our diagnostic setup.

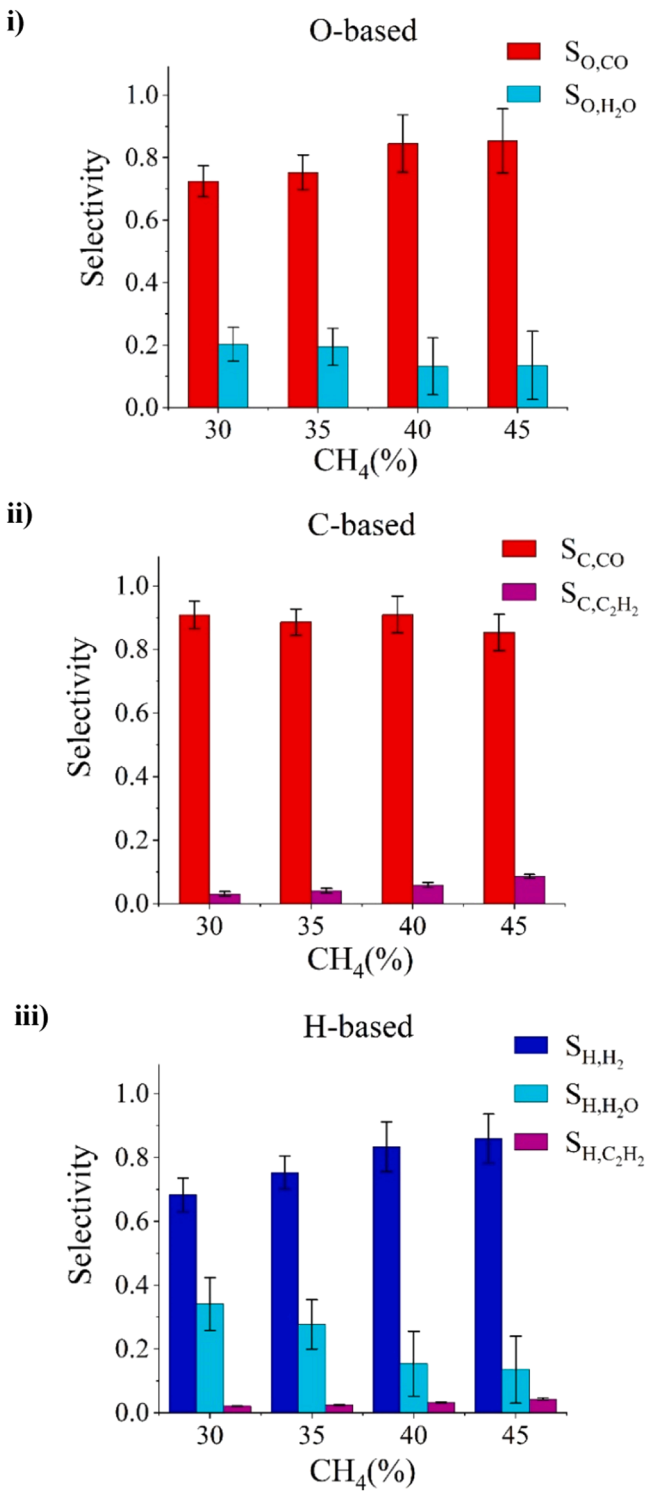

Fig. 4. Selectivity of O-, C- and H-based atoms towards the main DRM products (see Eqs. E12-E18) measured for the different CH_4 fractions in the CH_4/CO_2 inlet mixtures (x-axis) at 10 L/min total inlet mass flow rate and 1 kW power: **i)** selectivity of O atoms towards CO and H_2O. **ii)** selectivity of C atoms towards CO and C_2H_2. **iii)** selectivity of H atoms towards H_2, H_2O and C_2H_2.

In Fig. 4 iii) the H-based selectivity towards H_2, H_2O and C_2H_2 for the different inlet mixtures is given. At a 70/30 CO_2/CH_4 inlet mixture, the H-atom selectivity is $S_{H,H_2} = 0.68 \pm 0.05$, $S_{H,H_2O} = 0.34 \pm 0.08$ and $S_{H,C_2H_2} = 0.021 \pm 0.002$, while at 55/45 CO_2/CH_4 we find a re-distribution towards H_2 with $S_{H,H_2} = 0.86 \pm 0.08$, $S_{H,H_2O} = 0.14 \pm 0.10$ and $S_{H,C_2H_2} = 0.043 \pm 0.004$. The cumulative selectivity is typically ~1 across the range here (considering the relatively large error) with values of 1.04 ± 0.10 at 70/30 CO_2/CH_4 and 1.04 ± 0.13 at 55/45 CO_2/CH_4. The H_2 selectivity increase with CH_4 fraction is consistent with the increasing dominance of the DRM reaction (i.e., reaction R1 above) over water formation (i.e., reactions R2–4 above). Further, this trend corroborates with the O-based selectivity shown in Fig. 4i).

3.4. Carbon formation

The production of small quantities of solid carbon, observed in the plasma region and coated on the quartz tube downstream, especially for the higher CH_4 fractions studied (see Fig. 1 ii and iii), has a pronounced impact on the plasma stability (i.e., dictating a minimum SEI for sustainment) and has consequences for downstream utilisation of the product stream (e.g., coking of catalyst bed, in case the latter would be added, in so-called post-plasma catalysis). Further, the carbon formation will eventually require downstream separation, and it is, therefore, very important to understand the size of the particulates and their basic morphology.

SEM and EDX is employed to determine the particle size distribution, purity and the basic structure and morphology of the produced carbon. The form factor of prepared carbon samples consists of nm-sized primary particles (or "nodules") arranged into sub-micron aggregates, as shown in Fig. 5i) [95]. The sampled material is found to be metal-free, as illustrated by the EDX spectrum in Fig. 5 ii). The main peak in the spectrum is coming from C, with smaller peaks attributed to O and Al from the support, Si and Al from the detector and microscope hardware and Cl from the solvent used. Indeed, this is expected given the 'electrodeless' characteristics of our surface MW reactor design (i.e., the plasma does not contact any metal surface). Manual SEM image analysis estimates a mean primary particle size of the smallest entities in the collected aggregates of ~21.0 ± 5.9 nm (see Fig. 5 iii).

Raman spectroscopy is an efficient and information-rich analytical technique when carbon-based materials are under investigation. In short, the most important bands are the D and G bands, respectively centred at around 1330 cm^{-1} and 1580 cm^{-1}, as depicted in Fig. 6i). The D band in Raman spectroscopy corresponds to the breathing modes of carbon atoms in disordered or defect-induced structures, and it is associated with structural defects. At the same time, the G maximum in a Raman spectrum of a carbon-based material corresponds to the in-plane vibrations of carbon atoms and is associated with C-C bond stretching. The similar intensity for the D and G bands could indicate the presence of amorphous carbon, disordered graphite, or a highly defective carbon structure. Moreover, the absence of significant intensity difference between the D and G peaks suggests a lack of long-range order or a higher degree of structural disorder in the carbon black obtained material. The very weak 2D band also suggests the formation of amorphous or disordered carbon material at 2650–2700 cm^{-1}, characteristic of crystalline carbon materials. In many cases of amorphous or disordered carbon materials, the 2D band may be entirely absent or appear as a very weak band [96–98].

Thermogravimetric analysis of the residual carbon shows two distinct mass weight loss regions, as depicted in Fig. 6 ii. The first one, below 200 °C, may be correlated with the presence of limited volatile molecules (roughly 2%), most likely water. The second and most important one describes the thermal decomposition and oxidation processes of the carbon material (approx. 93%). The temperature interval of this consistent mass loss was observed between 400 °C and 650 °C, after which around 5% of the sample is left. The remaining carbon is stable until 1000 °C. It is rather difficult to pinpoint the nature of this residual, which can be in the form of crystalline carbon, carbonaceous particles, or other carbon-based structures that are more stable at high temperatures. Considering the relatively lower decomposition temperature of the carbon material (below 650 °C), we can conclude that the carbon is

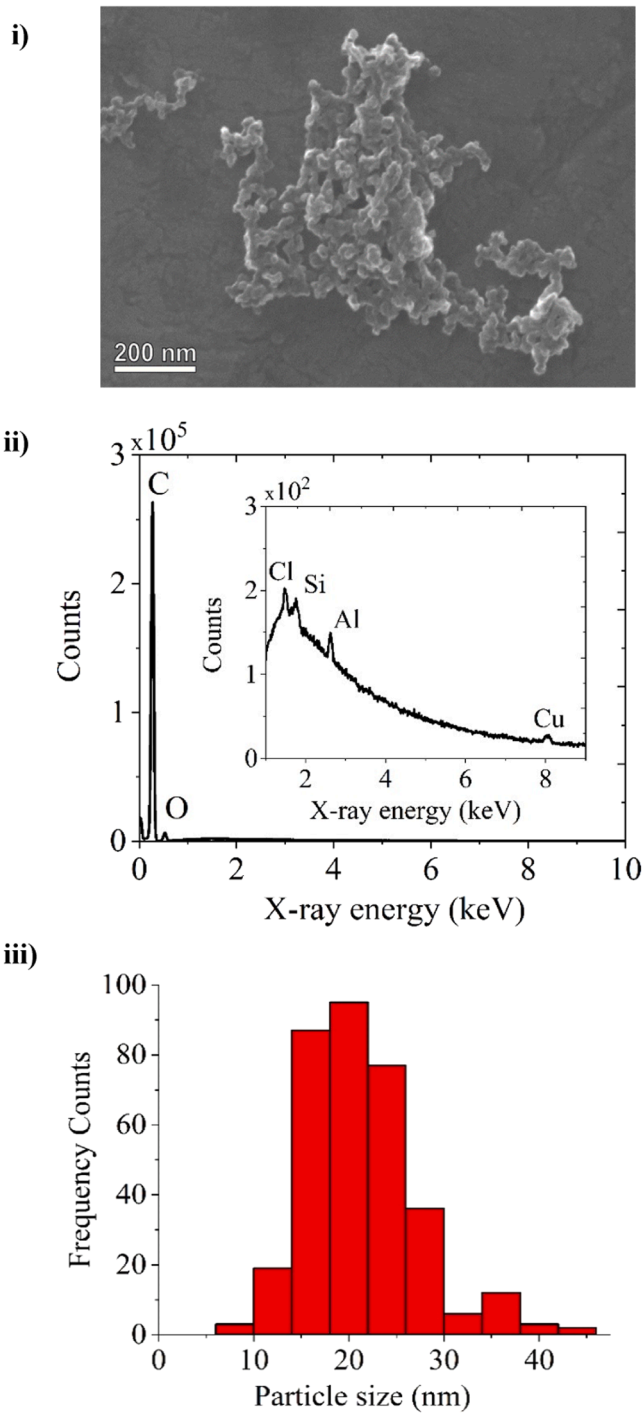

Fig. 5. i) SEM image of the carbon particles. Small nanoparticles are clustered together forming larger agglomerates. **ii)** Elemental analysis of the carbon particles using EDX. The main peak in the spectrum is coming from C, with smaller peaks attributed to O and Al from the support, Si and Al from the detector and microscope hardware, and Cl from the solvent used. The sampled carbon is found to be free of metal contaminants. **iii)** Particle size distribution of the carbon particles based on SEM images. The average particle size is 21.0 ± 5.9 nm.

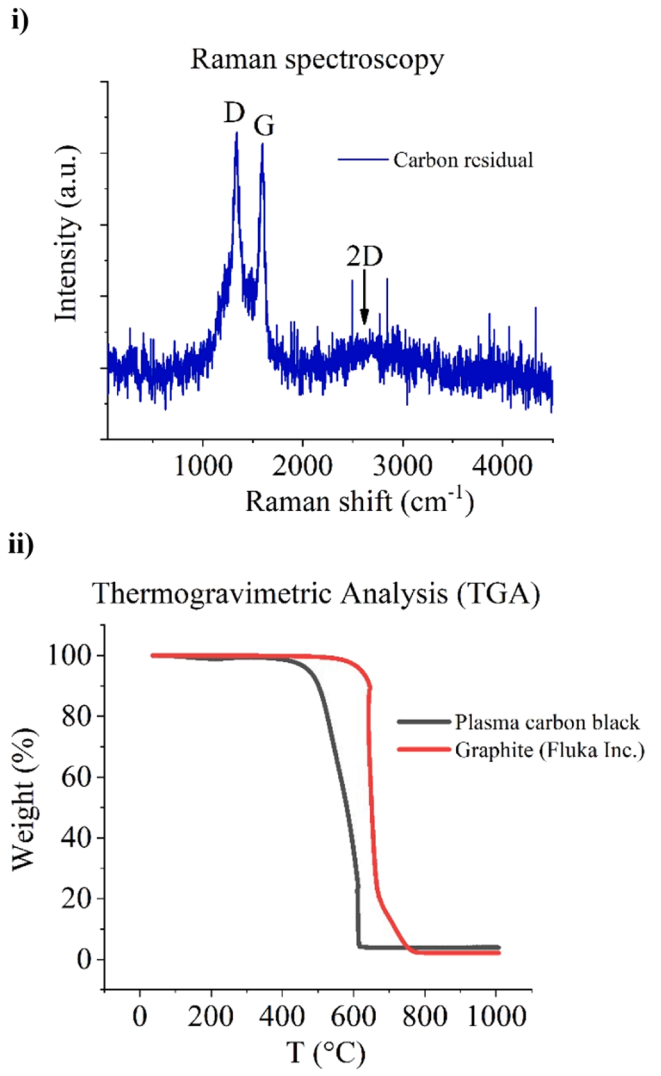

Fig. 6. : i) Raman spectrum of the plasma produced carbon material. Measurements performed using a green 532 nm laser at room temperature and in air atmosphere in the range of 50–4500 cm^{-1} Raman shift. **ii)** TGA profile of the plasma produced carbon material including a comparison with graphite powder (Fluka Inc., particle diameter of $\leq$ 20 μm). The measurement is performed in O_2 with a flow rate of 80 mL/min and temperature increase of 10 °C/min. until 1000 °C was reached.

amorphous and contains many structural defects [99]. Typically, crystalline carbon, e.g., in the form of graphite, is expected to burn at higher temperatures, even above 650 °C, as is confirmed in the TGA profile (see Fig. 6 ii). The amorphous structure of carbon makes it more reactive and susceptible to oxidation or combustion compared to crystalline carbon, which has a more ordered and stable structure. The increased reactivity of amorphous carbon is due to its higher surface area and structural defects, such as dangling bonds and disordered arrangements of carbon atoms [100,101].

In summary, the morphology and particle size distribution as observed by SEM and the largely amorphous structure of the carbon as indicated by the Raman and TGA measurements all support the hypothesis that the plasma-produced carbon particles resemble a 'carbon black' type material [102].

Carbon black is widely used as a filler in rubber and plastics where it promotes mechanical strength, durability and electrical conductivity [103]. Recovery/removal of particulates in gas flows can be carried out in a variety of ways, which include flow separation (e.g., cyclones) and electrostatic precipitators [104]. Notably, both methods are mature technologies for particulate separation at high temperatures (e.g., combustion flue gases) which could be advantageous to maintain the plasma exhaust thermal energy for downstream utilisation (e.g., heat exchange, catalyst bed). Evidently, the separated carbon black by-product could be a valuable commodity, lowering the overall cost of our MW plasma-based DRM process (e.g., offsetting the cost of carbon removal). The primary particle size is an important characteristic for the commercial attractiveness of carbon black materials, where (generally) smaller (primary) particle sizes are favoured as a filler for improving tensile strength, conductivity, specific surface area [105]. The range of particle sizes found here (i.e., 10–40 nm as shown in Fig. 5 iii)), for example, is consistent with a premium grade 'carbon black' used to reinforce rubber in abrasion-resistant automotive tyres [106].

3.5. Exhaust temperature

MW plasmas direct a considerable amount of the energy to heat (i.e., so-called warm plasma conditions) in addition to chemical energy used in converting the feed mixture. Utilisation of this 'waste' heat could lead to further improvement in the energy cost of the process. The utilisation of this 'hot exhaust' also strongly motivates investigation of coupling with downstream catalyst beds and heat/energy recovery configurations. Notably, effective strategies for carbon removal or coke-resistant catalysts will be required, with work on-going [107,108]. Such a study is beyond the scope of this work, however, to assess the potential for future progress, we recorded gas temperatures at a short distance outside the plasma region.

K-type thermocouples were placed downstream, in the exhaust plume, at ~15 cm from the outlet. The exhaust reaches a steady-state after approximately 15 min operation [79] when data is acquired. At a 70/30 CO_2/CH_4 inlet mixture, the gas temperature reaches 726 ± 9 K; at 60/40 CO_2/CH_4, it reaches 687 ± 5 K; and for 55/45 CO_2/CH_4 it reaches 677 ± 8 K. This shows a slight downward trend with increasing CH_4 fraction (and the increasing production and heating of solid carbon), with typical (average) values of ~700 K across the range. These conditions are at the lower end of activation temperatures required for thermal DRM catalysts [108]. Evidently, considerably higher exhaust temperatures occur at $<$ 15 cm (e.g., observation of the white incandescent carbon particulates characteristic with temperatures $>$ 1500 K), however, to avoid strong (electrical) coupling between the plasma and our thermocouple, we used a 'safe distance' here. Higher SEI, thermal insulation, and greater proximity ($<$ 15 cm) to the plasma would clearly benefit full exploitation of the heated exhaust for future plasma-catalytic reforming. However, this should be balanced against any possible disruptions to the swirling flow, plasma, and carbon production via the inclusion of a nearby catalyst bed.

4. Conclusion

In this paper, we investigate atmospheric pressure MW plasma conversion of CO_2 and CH_4 (i.e., dry reforming of methane, DRM) for different mixture fractions. This work gives original insight into the role of solid carbon on MW plasma-based DRM, a critical aspect which has not been studied in detail before. Further to this, for the first time, an estimation of the H_2O by-product levels in the exhaust is carried out via an atom balance analysis in the context of MW plasma-based DRM.

We achieve a total (weighted) conversion of ~50–53%, with a promising energy cost of ~2.8–3.0 eV/molecule (or ~11.1–11.9 kJ/L) with a syngas ratio of ~1 achieved at 45% CH_4. This performance is among the best when compared to the current state-of-the-art for plasma-based DRM for all types of plasma reactors reported in the literature, demonstrating the importance of the MW approach, which has the key benefit of being "electrodeless" (i.e., advantageous in limiting energy loss to, and erosion of, metallic electrodes, which may happen in other reactor designs).

Syngas (i.e., CO and H_2) is observed as the primary product of

conversion. The plasma shows distinct operation modes: for low CH_4 fractions (e.g., 70/30 CO_2/CH_4), a considerable H_2O by-product is formed (up to ~14%), but the discharge is relatively free of carbon formation. At higher CH_4 fractions (i.e., 55/45 CO_2/CH_4), H_2O production slightly decreases with a greater selectivity towards syngas production (CO and H_2) and syngas ratios ~1 at the output. Notably, the plasma filament is observed to become laden with carbon particles at higher CH_4 fractions (> 30%). At 50/50 CO_2/CH_4 mixtures, the plasma is unstable and quickly (< 10 s) extinguishes for our reactor conditions (10 L/min, 1 kW, SEI ~6 kJ/L). We believe this is the result of increasing carbon formation at higher CH_4 fractions and is evidenced by the considerable increase in luminosity observed from the plasma region. Characterisation of the solid carbon particles shows a 'carbon black' type material, consisting of pure, largely amorphous, carbon with a mean particle size of 20 nm.

Evidently, MW plasma-based DRM is considerably impacted by solid carbon formation, despite its relatively low production compared to the main products (i.e., H_2, CO and H_2O). A greater recognition of the role of solid carbon in plasma-based DRM is underlined in this work. Indeed, understanding the impact of carbon formation, especially at high CH_4 inputs, will be needed to drive technology readiness. This seems particularly relevant to reforming of biogas feedstocks (i.e., where CH_4 > 50%) and for Fischer-Tropsch processes and methanol production, requiring higher syngas ratios (i.e., H_2 / CO ratio ~ 2).

CRediT authorship contribution statement

Seán Kelly: Conceptualization, Methodology, Investigation, Writing – original draft. **Elizabeth Mercer**: Investigation of plasma aspects, Writing. **Robin De Meyer**: Investigation of carbon materials, Writing. **Radu-George Ciocarlan**: Investigation of carbon materials, Writing. **Sara Bals**: Supervision of carbon materials characterisation, Writing – review & editing. **Annemie Bogaerts:** Conceptualization, Supervision, Writing.

Declaration of Competing Interest

The authors declare that they have no known competing financial interests or personal relationships that could have appeared to influence the work reported in this paper.

Data Availability

Data will be made available on request.

Acknowledgements

We acknowledge financial support by a European Space Agency (ESA) Open Science Innovation Platform study (contract no. 4000137001/21/NL/GLC/ov), the European Marie Skłodowska-Curie Individual Fellowship "PENFIX'' within Horizon 2020 (grant no. 838181), the European Research Council (ERC) under the European Union's Horizon 2020 Research and Innovation Program (grant no. 810182; SCOPE ERC Synergy project), the Excellence of Science FWO-FNRS PLASyntH2 project (FWO grant no. G0I1822N and EOS no. 4000751) and the Methusalem project of the University of Antwerp.

References

[1] D.S. Mallapragada, Y. Dvorkin, M.A. Modestino, D.V. Esposito, W.A. Smith, B.-M. Hodge, M.P. Harold, V.M. Donnelly, A. Nuz, C. Bloomquist, K. Baker, L. C. Grabow, Y. Yan, N.N. Rajput, R.L. Hartman, E.J. Biddinger, E.S. Aydil, A. D. Taylor, Decarbonization of the chemical industry through electrification: Barriers and opportunities, Joule 7 (2023) 23–41.
[2] R. Snoeckx, A. Bogaerts, Plasma technology - a novel solution for CO_2 conversion? Chem. Soc. Rev. 46 (2017) 5805–5863.
[3] A. Bogaerts, E.C. Neyts, Plasma technology: an emerging technology for energy storage, ACS Energy Lett. 3 (2018) 1013–1027.
[4] IRENA, Global energy transformation: a roadmap to 2050 (2019 edition), Int. Renew. ENergy Agency (IRENA) (2019).
[5] H. Gladish, How fuels make acetylene by DC Arc, Hydrocarb. Process. Petrol. Refin. 41 (1962) 159–164.
[6] I.V. Bilera, Y.A. Lebedev, Plasma-chemical production of acetylene from hydrocarbons: history and current status (a review), Pet. Chem. 62 (2022) 329–351.
[7] B. Wanten, S. Maerivoet, C. Vantomme, J. Slaets, G. Trenchev, A. Bogaerts, Dry reforming of methane in an atmospheric pressure glow discharge: Confining the plasma to expand the performance, J. CO_2 Util. 56 (2022), 101869.
[8] A.P.H. Goede, CO_2-neutral fuels, EPJ Web Conf. 98 (2015) 07002.
[9] M. Rumayor, J. Fernández-González, A. Domínguez-Ramos, A. Irabien, Deep decarbonization of the cement sector: a prospective environmental assessment of CO_2 recycling to methanol, ACS Sustain. Chem. Eng. 10 (2022) 267–278.
[10] H.J. Venvik, J. Yang, Catalysis in microstructured reactors: Short review on small-scale syngas production and further conversion into methanol, DME and Fischer-Tropsch products, Catal. Today 285 (2017) 135–146.
[11] M. Loewert, J. Hoffmann, P. Piermartini, M. Selinsek, R. Dittmeyer, P. Pfeifer, Microstructured fischer-tropsch reactor scale-up and opportunities for decentralized application, Chem. Eng. Technol. 42 (2019) 2202–2214.
[12] X. Zhao, B. Joseph, J. Kuhn, S. Ozcan, Biogas reforming to syngas: a review, iScience 23 (2020), 101082.
[13] M. Banja, M. Jégard, V. Motola, R. Sikkema, Support for biogas in the EU electricity sector – a comparative analysis, Biomass-.-. Bioenergy 128 (2019), 105313.
[14] J. Zhang, Y. Yang, J. Zhang, Q. Liu, Study on the conversion of CH_4 and CO_2 using a pulsed microwave plasma under atmospheric pressure, Acta Chim. Sin. 60 (2002) 1973–1980.
[15] S.M. Chun, Y.C. Hong, D.H. Choi, Reforming of methane to syngas in a microwave plasma torch at atmospheric pressure, J. CO_2 Util. 19 (2017) 221–229.
[16] H. Sun, J. Lee, M.S. Bak, Experiments and modeling of atmospheric pressure microwave plasma reforming of a methane-carbon dioxide mixture, J. CO_2 Util. 46 (2021), 101464.
[17] S.M. Chun, D.H. Shin, S.H. Ma, G.W. Yang, Y.C. Hong, CO_2 microwave plasma—catalytic reactor for efficient reforming of methane to syngas, Catalysts 9 (2019) 292.
[18] W. Cho, W.-S. Ju, S.-H. Lee, Y.-S. Baek, Y.C. Kim, Investigation of synthesis gas production from natural gas and CO_2 by microwave plasma technology, in: S.-E. Park, J.-S. Chang, K.-W. Lee (Eds.), Studies in Surface Science and Catalysis, Elsevier, 2004, pp. 205–208.
[19] W. Bongers, H. Bouwmeester, B. Wolf, F. Peeters, S. Welzel, D. van den Bekerom, N. den Harder, A. Goede, M. Graswinckel, P.W. Groen, J. Kopecki, M. Leins, G. van Rooij, A. Schulz, M. Walker, R. van de Sanden, Plasma-driven dissociation of CO_2 for fuel synthesis, Plasma Process. Polym. 14 (2017) 1600126.
[20] N. den Harder, D.C.M. van den Bekerom, R.S. Al, M.F. Graswinckel, J. M. Palomares, F.J.J. Peeters, S. Ponduri, T. Minea, W.A. Bongers, M.C.M. van de Sanden, G.J. van Rooij, Homogeneous CO2conversion by microwave plasma: Wave propagation and diagnostics, Plasma Process. Polym. 14 (2017) 1600120.
[21] D.C.M. van den Bekerom, J.M.P. Linares, T. Verreycken, E.M. van Veldhuizen, S. Nijdam, G. Berden, W.A. Bongers, M.C.M. van de Sanden, G.J. van Rooij, The importance of thermal dissociation in CO_2 microwave discharges investigated by power pulsing and rotational Raman scattering, Plasma Sources Sci. Technol. 28 (2019), 055015.
[22] G.J. van Rooij, H.N. Akse, W.A. Bongers, M.C.M. van de Sanden, Plasma for electrification of chemical industry: a case study on CO2reduction, Plasma Phys. Control. Fusion 60 (2018), 014019.
[23] A.J. Wolf, T.W.H. Righart, F.J.J. Peeters, W.A. Bongers, M.C.M. van de Sanden, Implications of thermo-chemical instability on the contracted modes in CO_2 microwave plasmas, Plasma Sources Sci. Technol. 29 (2020), 025005.
[24] A.J. Wolf, T.W.H. Righart, F.J.J. Peeters, P.W.C. Groen, M.C.M. van de Sanden, W.A. Bongers, Characterization of CO_2 microwave plasma based on the phenomenon of skin-depth-limited contraction, Plasma Sources Sci. Technol. 28 (2019), 115022.
[25] G. Chen, N. Britun, T. Godfroid, V. Georgieva, R. Snyders, M.-P. Delplancke-Ogletree, An overview of CO_2 conversion in a microwave discharge: the role of plasma-catalysis, J. Phys. D: Appl. Phys. 50 (2017), 084001.
[26] G. Chen, L. Wang, T. Godfroid, R. Snyders, Progress in plasma-assisted catalysis for carbon dioxide reduction, in: B. Nikolay, S. Tiago (Eds.), Plasma Chemistry and Gas Conversion, IntechOpen, Rijeka, 2018. Ch. 4.
[27] T. Silva, N. Britun, T. Godfroid, R. Snyders, Optical characterization of a microwave pulsed discharge used for dissociation of CO_2, Plasma Sources Sci. Technol. 23 (2014), 025009.
[28] T. Silva, N. Britun, T. Godfroid, R. Snyders, Understanding CO_2 decomposition in microwave plasma by means of optical diagnostics, Plasma Process. Polym. 14 (2017) 1600103.
[29] F.A. D'Isa, E.A.D. Carbone, A. Hecimovic, U. Fantz, Performance analysis of a 2.45 GHz microwave plasma torch for CO_2 decomposition in gas swirl configuration, Plasma Sources Sci. Technol. 29 (2020), 105009.
[30] A. Hecimovic, F.A. D'Isa, E. Carbone, U. Fantz, Enhancement of CO_2 conversion in microwave plasmas using a nozzle in the effluent, J. CO_2 Util. 57 (2022), 101870.
[31] S. Soldatov, E. Carbone, A. Kuhn, G. Link, J. Jelonnek, R. Dittmeyer, A. Navarrete, Efficiency of a compact CO_2 coaxial plasma torch driven by ultrafast microwave power pulsing: Stability and plasma gas flow dynamics, J. CO_2 Util. 58 (2022), 101916.

[32] I. Belov, V. Vermeiren, S. Paulussen, A. Bogaerts, Carbon dioxide dissociation in a microwave plasma reactor operating in a wide pressure range and different gas inlet confurations, J. CO_2 Util. 24 (2018) 386–397.

[33] A. Berthelot, A. Bogaerts, Modeling of CO_2 splitting in a microwave plasma: how to improve the conversion and energy efficiency, J. Phys. Chem. C. 121 (2017) 8236–8251.

[34] S. Heijkers, R. Snoeckx, T. Kozák, T. Silva, T. Godfroid, N. Britun, R. Snyders, A. Bogaerts, CO2 Conversion in a Microwave plasma reactor in the presence of N2: elucidating the role of vibrational levels, J. Phys. Chem. C. 119 (2015) 12815–12828.

[35] T. Kozák, A. Bogaerts, Evaluation of the energy efficiency of CO2conversion in microwave discharges using a reaction kinetics model, Plasma Sources Sci. Technol. 24 (2014), 015024.

[36] V. Vermeiren, A. Bogaerts, Supersonic microwave plasma: potential and limitations for energy-efficient CO_2 conversion, J. Phys. Chem. C. 122 (2018) 25869–25881.

[37] V. Vermeiren, A. Bogaerts, Improving the energy efficiency of CO_2 conversion in nonequilibrium plasmas through pulsing, J. Phys. Chem. C. 123 (2019) 17650–17665.

[38] V. Vermeiren, A. Bogaerts, Plasma-based CO_2 conversion: to quench or not to quench? J. Phys. Chem. C. 124 (2020) 18401–18415.

[39] Y. Qin, G. Niu, X. Wang, D. Luo, Y. Duan, Status of CO_2 conversion using microwave plasma, J. CO_2 Util. 28 (2018) 283–291.

[40] E.R. Mercer, S. Van Alphen, C.F.A.M. van Deursen, T.W.H. Righart, W.A. Bongers, R. Snyders, A. Bogaerts, M.C.M. van de Sanden, F.J.J. Peeters, Post-plasma quenching to improve conversion and energy efficiency in a CO_2 microwave plasma, Fuel 334 (2023), 126734.

[41] F. Zhang, X. Zhang, Z. Song, X. Li, X. Zhao, J. Sun, Y. Mao, X. Wang, W. Wang, Promotion of microwave discharge over carbon catalysts for CO_2 reforming of CH4 to syngas, Fuel 331 (2023), 125914.

[42] N.M. Alawi, H.M. Nguyen, A. Barifcani, Optimization of microwave power, CO_2/CH4 ratio and total feed flow rate for the plasma dry reforming of methane, Iraqi J. Oil Gas. Res. (IJOGR) 1 (2021) 59–71.

[43] N.M. Alawi, G.H. Pham, A. Barifcani, Microwave plasma dry reforming of methane at high CO_2/CH4 feed ratio, Int. J. Chem. Mol. Eng. 13 (2019) 156–160.

[44] N.M. Alawi, G. Hung Pham, A. Barifcani, M. Hoang Nguyen, S. Liu, Syngas formation by dry and steam reforming of methane using microwave plasma technology, IOP Conf. Ser.: Mater. Sci. Eng. 579 (2019), 012022.

[45] S. Kreuznacht, M. Purcel, S. Böddeker, P. Awakowicz, W. Xia, M. Muhler, M. Böke, Av Keudell, Comparison of the performance of a microwave plasma torch and a gliding arc plasma for hydrogen production via methane pyrolysis, Plasma Process. Polym. 20 (2023) 2200132.

[46] S.I. Gritsinin, P.A. Gushchin, A.M. Davydov, E.V. Ivanov, I.A. Kossyi, M. A. Misakyan, Conversion of methane in a coaxial microwave torch, Plasma Phys. Rep. 35 (2009) 933–940.

[47] R. Vander Wal, A. Sengupta, E. Musselman, G. Skoptsov, Microwave-Driven Plasma-Mediated Methane Cracking: Product Carbon Characterization, C 4 (2018) 61.

[48] C. Shen, D. Sun, H. Yang, Methane coupling in microwave plasma under atmospheric pressure, J. Nat. Gas. Chem. 20 (2011) 449–456.

[49] J. Röpcke, L. Mechold, X. Duten, A. Rousseau, A time resolved laser study of hydrocarbon chemistry in H2-CH4 surface wave plasmas, J. Phys. D: Appl. Phys. 34 (2001) 2336.

[50] B. Hrycak, J. Mizeraczyk, D. Czylkowski, M. Dors, M. Budnarowska, M. Jasiński, Hydrogen production by the steam reforming of synthetic biogas in atmospheric-pressure microwave (915 MHz) plasma, Sci. Rep. 13 (2023) 2204.

[51] M. Jasiński, D. Czylkowski, B. Hrycak, M. Dors, J. Mizeraczyk, Atmospheric pressure microwave plasma source for hydrogen production, Int. J. Hydrog. Energy 38 (2013) 11473–11483.

[52] E. Cleiren, S. Heijkers, M. Ramakers, A. Bogaerts, Dry reforming of methane in a gliding arc plasmatron: towards a better understanding of the plasma chemistry, ChemSusChem 10 (2017) 4025–4036.

[53] K. Li, J.-L. Liu, X.-S. Li, H.-Y. Lian, X. Zhu, A. Bogaerts, A.-M. Zhu, Novel power-to-syngas concept for plasma catalytic reforming coupled with water electrolysis, Chem. Eng. J. 353 (2018) 297–304.

[54] J. Slaets, M. Aghaei, S. Ceulemans, S. Van Alphen, A. Bogaerts, CO_2 and CH4 conversion in "real" gas mixtures in a gliding arc plasmatron: how do N2 and O2 affect the performance? Green. Chem. 22 (2020) 1366–1377.

[55] D. Li, X. Li, M. Bai, X. Tao, S. Shang, X. Dai, Y. Yin, CO_2 reforming of CH4 by atmospheric pressure glow discharge plasma: A high conversion ability, Int. J. Hydrog. Energy 34 (2009) 308–313.

[56] X. Tao, M. Bai, X. Li, H. Long, S. Shang, Y. Yin, X. Dai, CH4–CO_2 reforming by plasma – challenges and opportunities, Prog. Energy Combust. Sci. 37 (2011) 113–124.

[57] D.K. Dinh, G. Trenchev, D.H. Lee, A. Bogaerts, Arc plasma reactor modification for enhancing performance of dry reforming of methane, J. CO_2 Util. 42 (2020), 101352.

[58] H. Kwon, T. Kim, S. Song, Dry reforming of methane in a rotating gliding arc plasma: Improving efficiency and syngas cost by quenching product gas, J. CO_2 Util. 70 (2023), 102448.

[59] H. Zhang, L. Li, X. Li, W. Wang, J. Yan, X. Tu, Warm plasma activation of CO_2 in a rotating gliding arc discharge reactor, J. CO_2 Util. 27 (2018) 472–479.

[60] H. Zhang, F. Zhu, X. Tu, Z. Bo, K. Cen, X. Li, Characteristics of atmospheric pressure rotating gliding arc plasmas, Plasma Sci. Technol. 18 (2016) 473–477.

[61] A. Wu, J. Yan, H. Zhang, M. Zhang, C. Du, X. Li, Study of the dry methane reforming process using a rotating gliding arc reactor, Int. J. Hydrog. Energy 39 (2014) 17656–17670.

[62] J.-L. Liu, H.-W. Park, W.-J. Chung, D.-W. Park, High-efficient conversion of CO_2 in AC-pulsed tornado gliding arc plasma, Plasma Chem. Plasma Process. 36 (2016) 437–449.

[63] A. Ozkan, T. Dufour, G. Arnoult, P. De Keyzer, A. Bogaerts, F. Reniers, CO_2–CH4 conversion and syngas formation at atmospheric pressure using a multi-electrode dielectric barrier discharge, J. CO_2 Util. 9 (2015) 74–81.

[64] X. Hu, Y. Liu, L. Dou, C. Zhang, S. Zhang, Y. Gao, X. Tu, T. Shao, Plasma enhanced anti-coking performance of Pd/CeO2 catalysts for the conversion of methane, Sustain. Energy Fuels 6 (2022) 98–109.

[65] X. Wang, Y. Gao, S. Zhang, H. Sun, J. Li, T. Shao, Nanosecond pulsed plasma assisted dry reforming of CH4: The effect of plasma operating parameters, Appl. Energy 243 (2019) 132–144.

[66] W.-Z. Jia, Q.-Z. Zhang, X.-F. Wang, Y.-H. Song, Y.-Y. Zhang, Y.-N. Wang, Effect of dust particle size on the plasma characteristics in a radio frequency capacitively coupled silane plasma, J. Phys. D: Appl. Phys. 52 (2019), 015206.

[67] N.H. Abuyazid, X. Chen, D. Mariotti, P. Maguire, C.J. Hogan, R.M. Sankaran, Understanding the depletion of electrons in dusty plasmas at atmospheric pressure, Plasma Sources Sci. Technol. 29 (2020), 075011.

[68] K. Dimoff, P.R. Smy, Dust induced quenching of an afterglow plasma, Phys. Lett. A 32 (1970) 13–14.

[69] M.I. Boulos, P. Fauchais, E. Pfender, High-power plasma torches and transferred arcs, in: M.I. Boulos, P.L. Fauchais, E. Pfender (Eds.), Handbook of Thermal Plasmas, Springer International Publishing, Cham, 2016, pp. 1–55.

[70] S.B. Shenoy, A. Rabinovich, A. Fridman, H. Pearlman, Process optimization of methane reforming to syngas using Gliding Arc Plasmatron, Plasma Process. Polym. 16 (2019) 1800159.

[71] D.H. Lee, 12 - Hydrogen production via the Kværner process and plasma reforming, in: V. Subramani, A. Basile, T.N. Veziroğlu (Eds.), Compendium of Hydrogen Energy, Woodhead Publishing, Oxford, 2015, pp. 349–391.

[72] V. Bilik, Six-Port Measurement technique: principles, impact, applications. https://s-team.sk/docs/SixPortTechnique.pdf, Invited paper at the Radioelektronika-2002 Conference, Bratislava, Slovakia, 14–16 May 2002, S-TEAM lab, https://s-team.sk/docs/SixPortTechnique.pdf, 2002.

[73] B. S-Team Lab, Sklovakia, HOMER-series STHT 2.45 GHz Autotuner with intergrated automatic impedance and power measurement system combined with a motorized 3 stub tuner. https://www.s-team.sk/products/autotuners, https://www.s-team.sk/products/autotuners, 2021.

[74] M. Moisan, C.M. Ferreira, Y. Hajlaoui, D. Henry, J. Hubert, R. Pantel, A. Ricard, Z. Zakrzewski, Properties and applications of surface wave produced plasmas, Rev. De. Phys. Appliquée 17 (1982) 707–727.

[75] M. Moisan, J. Pelletier, Physics of collisional plasmas. Application to high frequency discharges; physique des plasmas collisionnels. Application aux decharges haute frequence, Springer, France, 2006.

[76] S. Kelly, A. Bogaerts, Nitrogen fixation in an electrode-free microwave plasma, Joule 5 (2021) 3006–3030.

[77] Emerson Rosemount™ X-STREAM X2GP Continuous Gas Analyzer, https://www.emerson.com/en-us/catalog/rosemount-x-stream-x2gp-continuous-gas-analyzer, https://www.emerson.com/en-us/catalog/rosemount-x-stream-x2gp-continuous-gas-analyzer, 2020.

[78] PyroScience GmbH Firesting O2 sensor, https://www.pyroscience.com/en/, https://www.pyroscience.com/en/, 2021.

[79] S. Kelly, A. Bogaerts, Nitrogen fixation in an electrode-free microwave plasma Joule, Nitrogen Fixat. Electrode-Free Microw. Plasma, Accept. 5 (2021) (2021) 3006–3030.

[80] N. Pinhão, A. Moura, J.B. Branco, J. Neves, Influence of gas expansion on process parameters in non-thermal plasma plug-flow reactors: a study applied to dry reforming of methane, Int. J. Hydrog. Energy 41 (2016) 9245–9255.

[81] R. Snoeckx, A. Bogaerts, Plasma technology – a novel solution for CO_2 conversion? Chem. Soc. Rev. 46 (2017) 5805–5863.

[82] F. Girard-Sahun, O. Biondo, G. Trenchev, G. van Rooij, A. Bogaerts, Carbon bed post-plasma to enhance the CO_2 conversion and remove O2 from the product stream, Chem. Eng. J. 442 (2022), 136268.

[83] B. Wanten, R. Vertongen, R. De Meyer, A. Bogaerts, Plasma-based CO_2 conversion: how to correctly analyze the performance? J. Energy Chem. (2023).

[84] Electron Microscopy for Material Science (EMAT), Universiteit Antwerpen, https://www.uantwerpen.be/en/research-groups/emat/research/instrumentation/, 2023.

[85] M. Scapinello, E. Delikonstantis, G.D. Stefanidis, The panorama of plasma-assisted non-oxidative methane reforming, Chem. Eng. Process.: Process.Intensif. 117 (2017) 120–140.

[86] Pyrometry: A Practical Treatise on the Measurement of High Temperatures, Nature 106 (1920) 371–371.

[87] L.A.C. Klujszo, M. Rafaelof, R.K. Rajamani, Dust collection performance of a swirl air cleaner, Powder Technol. 103 (1999) 130–138.

[88] F. Ruiz-Perez, S.M. López-Estrada, R.V. Tolentino-Hernández, F. Caballero-Briones, Carbon-based radar absorbing materials: a critical review, Journal of Science: Advanced Materials and Devices 7 (2022), 100454.

[89] H.S. Uhm, Y.C. Hong, D.H. Shin, A microwave plasma torch and its applications, Plasma Sources Sci. Technol. 15 (2006) S26.

[90] Q. Wang, B.-H. Yan, Y. Jin, Y. Cheng, Investigation of dry reforming of methane in a dielectric barrier discharge reactor, Plasma Chem. Plasma Process. 29 (2009) 217–228.

[91] R. Snoeckx, Y.X. Zeng, X. Tu, A. Bogaerts, Plasma-based dry reforming: improving the conversion and energy efficiency in a dielectric barrier discharge, RSC Adv. 5 (2015) 29799–29808.
[92] T. Nunnally, K. Gutsol, A. Rabinovich, A. Fridman, A. Gutsol, A. Kemoun, Dissociation of CO2in a low current gliding arc plasmatron, J. Phys. D: Appl. Phys. 44 (2011), 274009.
[93] W.-C. Chung, M.-B. Chang, Dry reforming of methane by combined spark discharge with a ferroelectric, Energy Convers. Manag. 124 (2016) 305–314.
[94] S. Böddeker, V. Bracht, P. Hermanns, S. Gröger, F. Kogelheide, N. Bibinov, P. Awakowicz, Anode spots of low current gliding arc plasmatron, Plasma Sources Sci. Technol. 29 (2020) 08LT01.
[95] W. Peukert, C. Wadenpohl, Industrial separation of fine particles with difficult dust properties, Powder Technol. 118 (2001) 136–148.
[96] L. Pacquets, J. Van den Hoek, D. Arenas-Esteban, R.-G. Ciocarlan, P. Cool, K. Baert, T. Hauffman, N. Daems, S. Bals, T. Breugelmans, Use of nanoscale carbon layers on Ag-based gas diffusion electrodes to promote CO production, ACS Appl. Nano Mater. 5 (2022) 7723–7732.
[97] M. Pawlyta, J.-N. Rouzaud, S. Duber, Raman microspectroscopy characterization of carbon blacks: spectral analysis and structural information, Carbon 84 (2015) 479–490.
[98] Z. Li, L. Deng, I.A. Kinloch, R.J. Young, Raman spectroscopy of carbon materials and their composites: Graphene, nanotubes and fibres, Prog. Mater. Sci. 135 (2023), 101089.
[99] H.N. Sharma, L. Pahalagedara, A. Joshi, S.L. Suib, A.B. Mhadeshwar, Experimental study of carbon black and diesel engine soot oxidation kinetics using thermogravimetric analysis, Energy Fuels 26 (2012) 5613–5625.
[100] D. Losic, F. Farivar, P.L. Yap, A. Karami, Accounting carbonaceous counterfeits in graphene materials using the thermogravimetric analysis (TGA) approach, Anal. Chem. 93 (2021) 11859–11867.
[101] A. Naseri, A.D. Sediako, F. Liu, M. Barati, R.D. Baker, M.J. Thomson, In-situ studies of O2 and O radical oxidation of carbon black using thermogravimetric analysis and environmental transmission electron microscopy, Carbon 156 (2020) 299–308.
[102] C.M. Long, M.A. Nascarella, P.A. Valberg, Carbon black vs. black carbon and other airborne materials containing elemental carbon: physical and chemical distinctions, Environ. Pollut. 181 (2013) 271–286.
[103] E. Guth, Theory of filler reinforcement, Rubber Chem. Technol. 18 (1945) 596–604.
[104] J. Seville, Gas cleaning in demanding applications, Springer Science & Business Media, 2013.
[105] M. Bera, P. Gupta, P.K. Maji, Structural/load-bearing characteristics of polymer–carbon composites, in: M. Rahaman, D. Khastgir, A.K. Aldalbahi (Eds.), Carbon-Containing Polymer Composites, Springer Singapore, Singapore, 2019, pp. 457–502.
[106] Y. Fan, G.D. Fowler, M. Zhao, The past, present and future of carbon black as a rubber reinforcing filler – a review, J. Clean. Prod. 247 (2020), 119115.
[107] A. Bogaerts, X. Tu, J.C. Whitehead, G. Centi, L. Lefferts, O. Guaitella, F. Azzolina-Jury, H.-H. Kim, A.B. Murphy, W.F. Schneider, T. Nozaki, J.C. Hicks, A. Rousseau, F. Thevenet, A. Khacef, M. Carreon, The 2020 plasma catalysis roadmap, J. Phys. D: Appl. Phys. 53 (2020), 443001.
[108] L. Huang, D. Li, D. Tian, L. Jiang, Z. Li, H. Wang, K. Li, Optimization of Ni-based catalysts for dry reforming of methane via alloy design: a review, Energy Fuels 36 (2022) 5102–5151.